Improved printability and electrical conductivity of carbon black polymer composite with a customized nozzle of material extrusion process

Sarah Marion, T. Joffre, J. Jaxel, Franck Pigeonneau

▶ **To cite this version:**

HAL Id: emse-04488691
https://hal-emse.ccsd.cnrs.fr/emse-04488691

Submitted on 5 Mar 2024

Improved printability and electrical conductivity of carbon black polymer composite with a customized nozzle of material extrusion process

S. Marion[a,b], T. Joffre[d], J. Jaxel[c], F. Pigeonneau[a,*]

[a]*MINES Paris, PSL University, CEMEF - Centre for material forming, CNRS UMR 7635, CS 10207, rue Claude Daunesse 06904 Sophia Antipolis Cedex, France*
[b]*Mines Saint-Etienne, Univ. Lyon, CNRS, UMR 5307 LGF, Centre SMS, 42023 Saint-Etienne, France*
[c]*MINES Paris, PSL University, Centre for processes, renewable energies and energy systems, CS 10207, rue Claude Daunesse 06904 Sophia Antipolis Cedex, France*
[d]*IPC Innovation Plasturgie Composites, 2 rue Pierre & Marie Curie, 01100 Bellignat, France*

Abstract

Due to the interactions between the fillers, the polymer and the die, the printing of filled polymer composites using the material extrusion process is challenging. Numerical computations have been carried out to investigate the fluid dynamics and heat transfer within the hot end of the material extrusion process. Firstly, a standard nozzle equipping the majority of 3D printers is considered. However, it is not possible to print an object on a commercial printer with a composite made of polylactic acid with $12\,\mathrm{wt\%}$ of carbon black due to clogging issues. This impossibility is supported by the application of the Q-criterion, which is an indicator of flow kinematics. As a result, a novel nozzle design is proposed. The printing of the same object on the same printer equipped with the new nozzle succeeds. The electrical properties of walls printed with both the standard and the new nozzles are evaluated. The conductivity of a wall printed with the new nozzle is $42\,\%$ higher than that of a wall printed with the standard nozzle. Furthermore, complementary analysis using scanning electron microscopy shows that the porosity of the walls printed with the new nozzle is reduced which is a promising improvement.

Keywords: material extrusion process, filled polymer, electrical conductivity, nozzle design

*Corresponding author: Tel. +33 (4) 93 95 74 34.
Email address: `franck.pigeonneau@minesparis.psl.eu` (F. Pigeonneau)

1. Introduction

Additive manufacturing encompasses a large family of processes for the printing of objects by adding material layer by layer. The most widely used technique in polymer additive manufacturing is the fused filament fabrication (FFF) or material extrusion process [1]. This process consists of depositing polymer threads in successive layers from a hot-end extruder. The product is designed using CAD software. To build the printed object layer by layer, the object is cut into fine slices using software called a "slicer", which allows the writing in a G-code language to command the printer. Material extrusion offers a much wider choice of materials. A large number of thermoplastic polymers are now printable, ranging from commodity thermoplastics like poly(lactic acid) (PLA), acrylonitrile butadiene styrene (ABS), polylactic acid (PA) or polyethylene terephthalate glycol-modified (PETG) to high-performance polymers such as polyether ether ketone (PEEK), polyethyleneimine (PEI) or polyether ketone ketone (PEKK). In addition, the material extrusion process allows the printing of multiple materials on the same part, thanks to a multi-extrusion printer.

Polymers are known for their low electrical conductivity. For example, the resistivity of polystyrene is on the order of $10^{20}\,\Omega\,\mathrm{m}$. To enhance the electrical conductivity of a polymer, one technique is to introduce conductive particles into a thermoplastic polymer. The behavior between electrical resistivity and the rate of conductive charging is not linear [2]. When conductive charges are added, a sharp transition from the insulating to the conductive state is observed at a critical charge concentration. The inflection point on the electric conductivity curve called the percolation threshold, is used to describe the sharp increase in the electrical conductivity. The sharp increase in the electrical conductivity is explained by the creation of conductive pathways through the contacts between the particles and, at a macroscopic level, through the material.

By adding charges to the polymer matrix, the electrical conductivity of the composite can be increased by many orders of magnitude [3]. Carbon, stainless steel fibers, graphite, or graphene are currently used both to reinforce thermoplastic compounds and to improve the electrical and thermal conductivities of thermoplastics [4]. Carbon black (CB) is the most widely used additive to improve the electrical conductivity of polymers. CB are formed by aggregates of primary fused particles (of the order of 20 nm) joined together by

van der Waals forces [5]. As pointed out by Zhang et al. [6], the working parameters of the material extrusion process influence the overall conductivity of ABS/CB composite. The main reason is the degradation of CB during the processing. The layer thickness and the distance between threads affect the porosity and therefore the electrical conductivity of the printed object. Inevitably, parts printed by a material extrusion process are porous with a porosity between 2 and 20 %. A loss of conductivity between the filament and the final part is then expected.

These compounds are currently used to protect electronic components against electromagnetic fields in the aeronautical industry [4]. In addition, conductive polymers could allow electronic circuits to be integrated directly into products, eliminating the additional post-processing steps required in laser direct structuring (LDS) [7].

Short fiber reinforced materials are compatible with the FFF process since it is possible to make filaments from electrical conductive compounds. However, printing highly charged polymers (above 30 wt%) with a FFF printer remains a challenge because reinforcing particles can often cause nozzle clogging. Croom et al. [8] have studied the various mechanisms of nozzle clogging. They pinpointed that the occurrence of clogging correlates fiber volume fraction, fiber length, and nozzle geometry. Specific clogging mechanisms include the accumulation of disoriented fibers and the retention of fiber entanglement in the nozzle tip. To avoid clogging in the nozzle, Croom et al. [8] suggested a modified nozzle geometry with a smooth, monotonically tapered flow profile. Jang et al. [9] investigated the working conditions of the material extrusion process on the filament morphology and void occurrence for a high solid-loaded suspension. They pinpointed that the gap between the substrate and the nozzle is a key parameter for the porosity of the printed object.

Fiber orientation in the polymer melt is influenced by the flow field, including die convergence flow and extrudate swelling. According to Heller et al. [10], the convergence region and the extrudate swelling region have a large influence on the fiber orientation and the mechanical properties of short fiber suspensions in the polymer melt during the FFF processing. Kanarska et al. [11] numerically investigated the fiber orientation for different die geometries and fibers. When the ratio of fiber length to nozzle diameter is between 0.5 and 0.67, the fiber flow undergoes dramatic changes. Fibers begin to

concentrate at the edges of the die, resulting in a low concentration of fibers in the center of the die. The best fiber alignment is achieved with fiber lengths between 0.4 and 0.5 times the nozzle diameter.

Fallon et al. [12] reviewed the state-of-the-art of highly filled, continuous short fiber polymers for material extrusion additive manufacturing. According to Fallon et al., [12], the nozzle clogging would be due to excessive viscosity of the polymer melt and fiber accumulation at the nozzle outlet. In addition, the smaller the diameter of the die outlet, the lower the maximum viscosity.

Abdalla et al. [13] studied the effect of layer thickness on electrical conductivity. The electrical resistivity increases with layer thickness mainly due to the voids created between the printed layers during the FFF process. The number of these voids increases with layer thickness. These air-filled voids reduce the point-to-point contact area required to create conductive paths.

In the molten wire deposition technique, the crossing of the charge through the nozzle causes the dispersion of the charge. Today, it is impossible to predict this change in dispersion. Therefore, it is needed to measure the conductivity loss between the filament and the printed part. Only a few studies have been devoted to the effect of additive manufacturing parameters on the properties of electrostatic discharge (ESD) materials. Parameters such as fill pattern, temperature, and printing velocity can also affect ESD material properties. However, it is difficult to predict the influence of these parameters on the performance of ESD materials.

From this review, it is clear that the convergence inside the nozzle plays an important role in clogging. Consequently, the main objective of this contribution is to reduce the clogging of composite materials and to improve the electrical conductivity of printed objects. The work is divided into two parts. Firstly, a new nozzle is designed based on computational fluid dynamics, section 2. Secondly, after 3D building the new nozzle, the printability of a composite made of poly(lactic acid) with carbon black fillers (PLA/CB) is investigated by studying the microstructure, the porosity, and electric conductivity of simple printed walls obtained with a standard and the new nozzles.

In complement, **??** gathers the material properties required for numerical computations, and 5 details the derivation of the divergence of particle velocity.

2. Nozzle design by computational fluid dynamics

According to the work of Jones et al. [14], the extruder of the material extrusion process consists of a heat block heated by a thermistor. The polymer is pushed through the heat block by a mechanical device. To prevent the polymer from heating up outside the heat block, a heat sink with a fan is placed above the heat block. For greater efficiency, an air gap called a heat break, is also added between the heat block and the heat sink. Inside the heat block, the polymer is melted in a barrel. The extrusion is achieved through a nozzle that can be replaced by users. More details on the design of extruders can be found on the website [15]. To improve the roughness of the printing object, the size of the filament must be reduced. According to Xu et al. [16], the width and the height of a deposited filament are proportional to the exit diameter of the nozzles. To improve roughness, the nozzle diameter must be reduced. However, a nozzle that is too small can degrade printability by causing clogging issues and also reducing the welding between the threads. Nozzles have been designed with various diameters, see reference [15]. The main characteristic dimensions of standard nozzles have been reported in Figure 1a. Whatever the nozzle, L is equal to 12.5 mm. The barrel diameter, D, is equal to 2 mm when the polymer filament is set equal to 1.75 mm. The angle of the conic part is also constant whatever the exit diameter, d. According to [15], 2α is equal to $\pi/3$. The length ℓ of the capillary tube is defined as a function of the diameter d.

In order to obtain acceptable roughness and maintain printability d is set to 300 μm giving a capillary length set to ℓ=450 μm according to the design of the standard nozzles supplied in [15].

Before designing a new nozzle, numerical computations have been done on an extruder with a standard E3D-V6 nozzle. The analysis is focused on the thermal and pressure drop. Only the fluid flow and the thermal behaviors through the extruder are described. The geometry of the liquefier used for numerical computations is given in Figure 1b corresponding mainly to the heat block with the nozzle. This geometry is similar to the previous work [17]. The polymer is a PLA charged with carbon black. Characteristic dimensions are given in mm. The boundary of the liquefier comprises the inlet section $\partial\Omega_{\text{in}}$, the surface of the cylinder $\partial\Omega_{\text{cyl}}$, the cone and the capillary die surfaces of the nozzle $\partial\Omega_{\text{noz}}$ and the outlet section $\partial\Omega_{\text{out}}$. The polymer is introduced from the left side
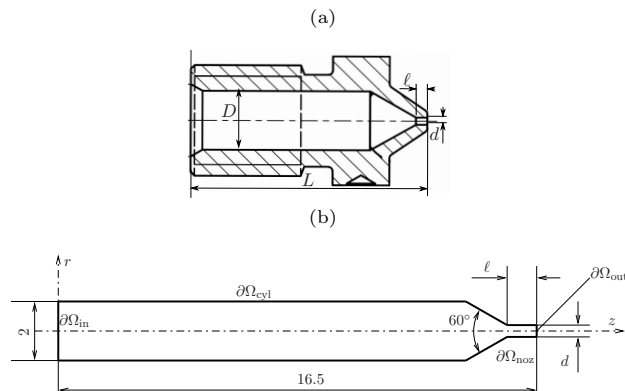
Figure 1: (a) Cross-section of a nozzle equipping the E3D-V6 extruder with d the exit diameter, ℓ the length of the capillary tube, $D{=}2\,\mathrm{mm}$ the inlet diameter and $L{=}16.5\,\mathrm{mm}$ the length of the nozzle; (b) Geometry of the computational domain corresponding to the interior of the heat-block with the nozzle. Dimensions are in mm. The total length of the domain takes into account the barrel and the nozzle.

and exits at the other extremity after extrusion through the nozzle.

Although an air gap exists between the polymer and the extruder barrel at the inlet, it disappears after a few tens of seconds. Marion et al. [17] have achieved a numerical study to investigate this phenomenon. The main mechanism underlying the disappearance of the air gap is the melting of the polymer in contact with the nozzle in the early stages. Due to the pressure on the filament, the polymer rises up along the nozzle and the barrel walls, ultimately eliminating the air gap. At large times, the air gap is either completely eliminated or is present only a few millimeters (see [17] for more information). As a result, the interior of the extruder is assumed to be entirely filled with polymer, and the fluid motion is assumed to be in a steady-state regime. The numerical method used in this study is not detailed here. For more information, the reader is referred to [17, 18].

Although an air gap between the polymer and the barrel of the extruder at the inlet, the air gap disappears after a few tens of seconds. This phenomenon has been studied numerically in [17]. The main mechanism explaining the disappearance of the air gap is due to the melting of the polymer a the contact of the nozzle at the early stages. Due to the pressure on the filament, the polymer rises up along the nozzle and the barrel walls leading to the removal of the air gap. At large times, the air gap is either fully removed or exists over a few millimeters (see for more details [17]. Consequently, the interior of the

extruder is assumed to be completely filled with polymer. The fluid motion is assumed in a steady-state regime. The numerical method is not detailed here (see references [17, 18] for more information).

2.1. Numerical results on the standard E3D-V6 nozzle

Thermal and mechanical properties required for numerical computations are provided in ??. The composite material is a carbon black-filled PLA (PLA/CB) with a chemical composition given in Table ??. The weight fraction of CB is equal to 21.43 wt%. A DSC analysis is used to set the glass transition temperature T_g and the melting temperature T_m. The specific heat capacity and characterization of the viscosity via rheology measurements were also carried out. The dynamic viscosity behaves like a pure polymer, with a Newtonian plateau and shear-thinning behavior at high shear flow. At first glance, the PLA/CB composite is assumed to obey a generalized Newtonian fluid. The PLA matrix is a semi-crystalline polymer. Latent heat release is expected during melting. Guo et al. [19] studied the electrical conductivity, mechanical properties, and thermal behaviors. While the enthalpy of reaction for pure and fully crystallized PLA is equal to $93.6 \times 10^3 \, \mathrm{J \, kg^{-1}}$, the addition of CB reduces the level of crystallization. When the weight fraction of CB is around 20 wt%, corresponding to our composite, the crystallinity is equal to 30 %. Guo et al. [19] found from their DSC measurements that the enthalpy of crystallization and that of melting are $20.3 \times 10^3 \, \mathrm{J \, kg^{-1}}$ and $22.53 \times 10^3 \, \mathrm{J \, kg^{-1}}$ respectively. With the heat capacity given in ??, the decrease or the increase in temperature is determined by the ratio of $\Delta H_r / C_p$ with ΔH_r the enthalpy of crystallization or of fusion. This ratio is smaller than 10 K. The melting temperature range given below is around $\Delta T = 200 \, \mathrm{K}$. Therefore, the heat produced by the chemical reaction accounts for only 5 % of the total heating. Consequently, the contributions of crystallization and fusion are neglected in the energy balance. The numerical computations have been achieved for three extrusion velocities U as defined by

$$U = \frac{4\dot{V}}{\pi d^2},\tag{1}$$

in which $\dot{V}$ is the volumetric flow rate. The inlet temperature is set at 20 °C , with the extruder temperature at 230 °C. Figure 2 presents the temperature field in the extruder for the three velocities equal to 25, 50 and 100 mm s^{-1}. The black solid line indicates
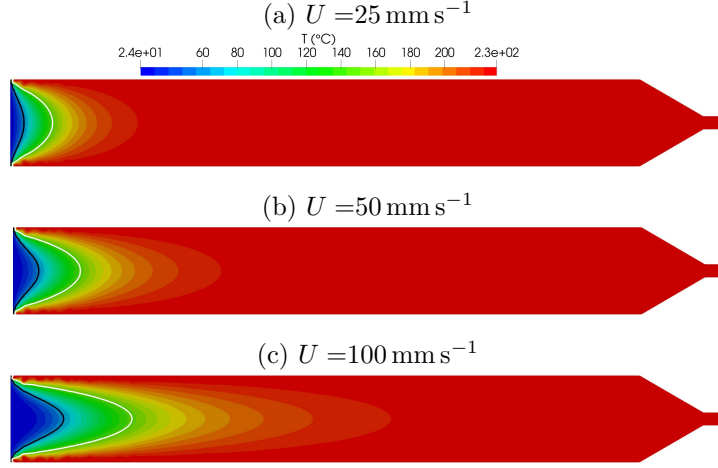
Figure 2: Temperature fields (°C) of the polymer in the symmetry plane in the extruder equipped with a standard E3D-V6 nozzle for three extrusion velocities.

the iso-T_g, while the white solid line represents the iso-T_m showing visually where the melting occurs. As expected the increase of the extruder velocity postpones the area where the melting occurs. The temperature on the nozzle remains uniform for the three conditions.

To control the pressure drop through the extruder, Figure 3 represents the dimensionless pressure as a function of the axial distance from the inlet to the outlet. The pressure is normalized by $\eta_0 U/D$ with η_0 the dynamic viscosity at low shear rate, U the extrusion velocity, and D the barrel diameter. The shear thinning is observed since with the increase of extrusion velocity, the pressure drop decreases mainly in the capillary tube of the nozzle. In both cases, the pressure drop in the first part of the extruder is less than in the nozzle comprising the convergent and the capillary tube.

For U=25, 50 and 100 mm s^{-1}, the feeding force obtained by the product of the inlet pressure and the cross-sectional area is equal to 1.55, 2.59 and 4.31 N, respectively.

To detect the presence of preferential concentrations of carbon black, the Q-criterion has been determined. For a solenoidal velocity field, the Q-criterion is defined as follows

$$Q = -\frac{1}{2}\operatorname{tr}(\boldsymbol{\nabla u} \cdot \boldsymbol{\nabla u}) = -\frac{u_{i,j}u_{j,i}}{2}, \tag{2}$$

where $u_{i,j}$ is the spatial derivative of the component u_i over the spatial coordinate. In the second equality, the Einstein convention of the repeated index is used. The
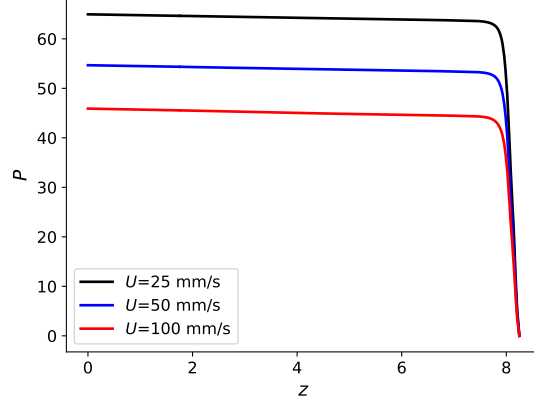
Figure 3: Dimensionless pressure as a function of normalized z for the three velocities in the extruder with a standard E3D-V6 nozzle. The coordinate z is normalized by D.

Q-criterion corresponds to the second invariant of the characteristic polynomial of the velocity gradient. Using the definition of the angular velocity [20]

$$\boldsymbol{\omega} = \frac{1}{2} \boldsymbol{\nabla} \times \boldsymbol{u}, \tag{3}$$

Q can also be written as follows

$$Q = \boldsymbol{\omega}^2 - \frac{1}{2} \operatorname{tr}(\dot{\boldsymbol{\epsilon}}^2), \tag{4}$$

meaning that irrotational flow areas have a negative Q value. Conversely, Q will be positive in the area of strong vorticity.

The sign of the Q-criterion gives information where the carbon black moves in greater concentration resulting in clogging. According to Elperin et al. [21], the preferential concentration of the particles can be evaluated by looking at the sign of the divergence of the particle velocity. Using the Stokes law applied to carbon black particles, the divergence of the particle velocity field is given by

$$\boldsymbol{\nabla} \cdot \boldsymbol{v}_p = 2\tau_p Q, \tag{5}$$

with τ_p is given by

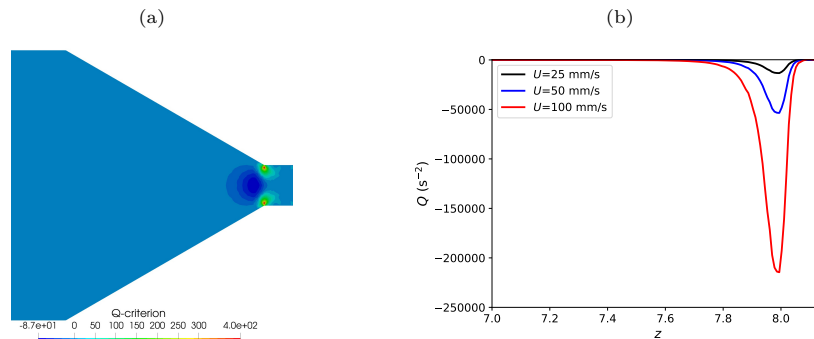$$\tau_p = \frac{2\rho_p r_p^2}{9\eta}, \tag{6}$$

Figure 4: (a) Q field at the end of the extruder with a standard E3D-V6 nozzle for $U{=}100\,\mathrm{mm\,s^{-1}}$; (b) Q $(\mathrm{s^{-2}})$ as a function of z at the end of the extruder with a standard E3D-V6 nozzle for the three cases.

with ρ_p the particle density, r_p the particle radius and η the dynamic viscosity of the molten polymer. This characteristic time is the ratio of the particle mass to the factor $6\pi\eta a$ coming from the Stokes law. The derivation of the equation (5) is given in 5.

Figure 4a shows the Q-criterion in the symmetric plane at the end of the extruder with a standard E3D-V6 nozzle. As the results in dimensionless units are similar for both velocities, only the case for which $U{=}100\,\mathrm{mm\,s^{-1}}$ is shown. Apart from the interaction of the convergent and the capillary tube, the Q-criterion is equal to zero, which means that the carbon black distribution should be uniform. At the junction of the convergent and the capillary, the Q-criterion is negative around the symmetry axis and near the inlet of the capillary tube. This would be the area where the black carbon could be in high concentration. At the edge of the junction of the convergent and the capillary tube, the Q-criterion takes the largest positive value.

Figure 4b shows Q on the symmetry axis as a function of z in the physical dimension, $\mathrm{s^{-2}}$, for the three cases. The magnitude of the Q-criterion increases with the square of U. Consequently, the probability of clogging is enhanced with the increase of the extrusion velocity. The first junction between the convergent and the main cylinder does not induce the generation of the Q-criterion because the shear rate is too low. Conversely, the presence of an edge in high shear regions leads to a strong Q-criterion.

A test on printing of a macroscopic object with a PLA/CB composite filament, presented in the next section, using a Prusa i3 MK3S 3D printer failed when a standard E3D-V6 was installed in the printer. This failure confirms our analysis based on the
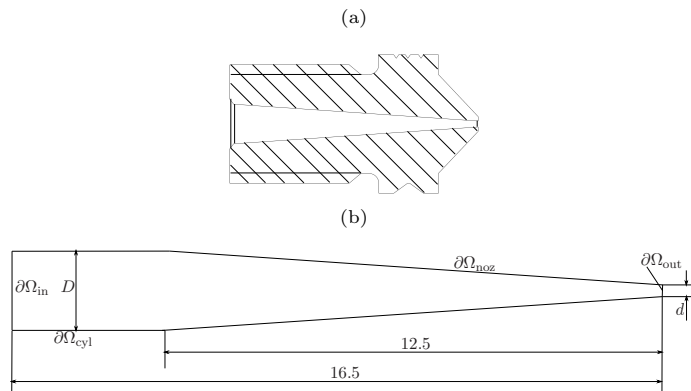
10

Figure 5: (a) Cross-section of the new nozzle with an outlet diameter of 300 µm and an inlet diameter of 2 mm; (b) Computational domain of the extruder with the new nozzle.

examination of the Q-criterion.

2.2. Numerical results with a new nozzle

A new nozzle has been designed to improve the printability of the charged polymer. To avoid the generation of vorticity through the extruder, the presence of an edge in the area of high shear rate, i.e., a small radius, has been eliminated. Figure 5a shows the cross-section of the new nozzle. As suggested by Croom et al. [8], the interior of the nozzle is formed by a unique cone reducing geometry singularities. The outlet diameter is set to 300 µm, while the inlet diameter is set to 2 mm. The other dimensions are the same as for the standard nozzle. In Figure 5b, the cross-section of the computational domain accounted for the heatblock and the nozzle is depicted. The barrel section is greatly reduced in this new design.

Numerical computations were carried out on the new geometry to check the effect of the change on temperature and fluid dynamics. As before, three extrusion velocities are used. The thermal condition is also the same. Figure 6 shows the temperature field in the symmetric plane for the three velocities. To control the temperature range in which the melting occurs, the solid black line corresponding to iso-T_g and the solid white line corresponding to iso-T_m are shown. As with the standard nozzle, the increase in velocity shifts the limit at which T_g is reached upwards. The spatial range between the two limits increases with the velocity.
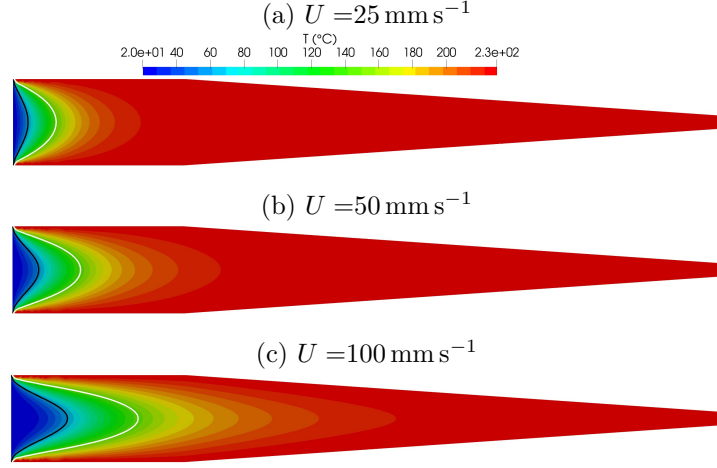
11

Figure 6: Temperature fields (°C) of the polymer in the symmetry plane in the extruder equipped with the new nozzle for three extrusion velocities.

The change in geometry has an effect on the pressure drop, as it can be seen in Figure 7 where the dimensionless pressure is plotted as a function of the z coordinate. The introduction of a unique cone increases the pressure drop. Shear thinning is also important in the new design. Using the characteristic pressure for normalization, the feeding forces can be estimated. For U=25, 50 and 100 mm s^{-1}, the feeding forces are equal to 2.36, 4.06 and 7.02 N respectively. The greatest increase is observed at the highest extrusion velocity for which the feeding force is 63 % more important than for the standard nozzle.

The evaluation of the Q-criterion inside the extruder with the new nozzle remains equal to zero throughout the computational domain. Consequently, no preferential concentrations of carbon black are expected.

To test the new design, a nozzle was manufactured by metal additive manufacturing using the SLM (Selective Laser Melting) process, which consists of successively melting layers of metal powders in a chamber under a controlled atmosphere, using an EOS M290 printer. The inside of the nozzle is machined using wire EDM by the Technifil company.

The new nozzle has been installed in a Prusa i3 MK3S 3D printer. The CAD image of an elliptical lid with a salamander shown in Figure 8a has been designed to test the impression with PLA/CB composite. The semi-major and the semi-minor axes of the
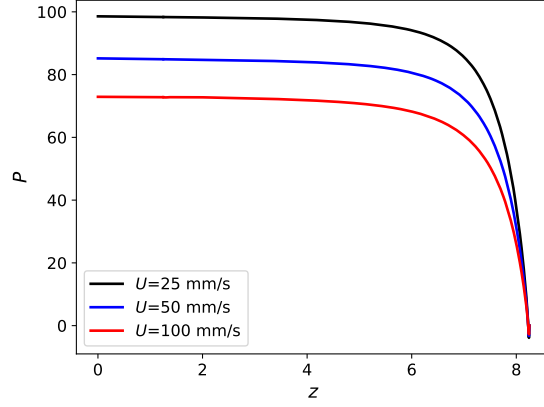
Figure 7: Dimensionless pressure as a function of normalized z for the three velocities in the extruder with the new nozzle.
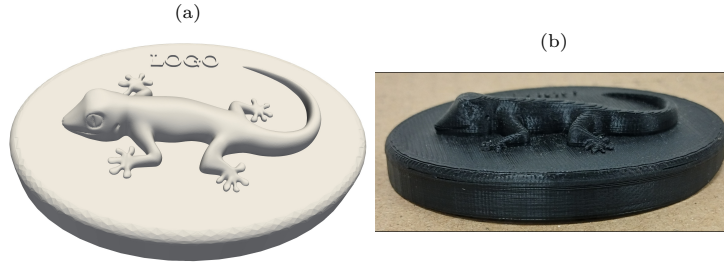

Figure 8: Lid with a salamander on the top: (a) CAD image obtained from the STL file, (b) photograph of the lid printed with the new nozzle on a Prusa i3 MK3S 3D printer.

elliptical part of the lid are equal to 35 and 25 mm respectively. The height of the lid is equal to 17.72 mm. While the impression with a standard E3D-V6 nozzle failed, the use of the new nozzle allowed the lid to be printed. Figure 8b is an image of the printed lid with the PLA/CB composite. Note also that even though the pressure drop is expected to be more important with the new nozzle, the printer never fails to extrude filament.

3. Electrical characterization of printed objects

Carbon black has been widely used as an additive in thermoplastic filaments to improve the electrical conductivity of printed objects, which is of particular interest for printing electronics or electromagnetic shielding. To test the electrical properties, thin

Table 1: Printing working conditions chosen to print walls of $100\times2\times1\,\text{mm}^3$.

V	T extruder	T plate	layer thickness
$20\,\text{mm}\,\text{s}^{-1}$	$230\,°\text{C}$	$60\,°\text{C}$	$10^{-1}\,\text{mm}$

Table 2: Values of the electrical properties according to the different nozzles.

Nozzle	Resistance (Ω)	Conductivity ($\text{S}\,\text{m}^{-1}$)
E3D-V6	2450	2.04
New	1730	2.89

walls of $100\times2\times1\,\text{mm}^3$ were printed. A Prusa i3 MK3S 3D printer is used to print samples using the PLA/CB filament. The main properties of the material are given in **??**. The printing working conditions are given in Table 1. The printing velocity, V, is set to $20\,\text{mm}\,\text{s}^{-1}$. The extruder temperature is set to $230\,°\text{C}$ while the heated bed temperature is set to $60\,°\text{C}$. Both standard E3D-V6 and the new nozzles were used to print these walls.

Electrical resistance measurements were carried out on the walls using the 2-point method with an ohmmeter. The electrical resistance of the PLA/CB is measured using the two-probe method and listed in Table 2 for the two walls. The electrical resistance of the wall printed with the new nozzle is $30\,\%$ lower than the wall printed with the E3D-V6 nozzle.

In addition to the printability improvement observed with the new nozzle, the electrical conductivity is also improved when the printer used the new nozzle which is one of the main achievements of our contribution.

3.1. Morphological analysis

A scanning electron microscope (SEM TESCAN Maia 3 Triglav) is used to study the morphology of the printed walls. In particular, the cross-section normal to the main printing direction is investigated. To obtain a surface as flat as possible, the samples are cut with a diamond blade. Before SEM observations, a layer of platinum of $7\,\text{µm}$ was deposited on some samples. An accelerating voltage of $3\,\text{kV}$ was applied to take the images. The whole cross-section of the strip is shown in Figure 9 with a SEM
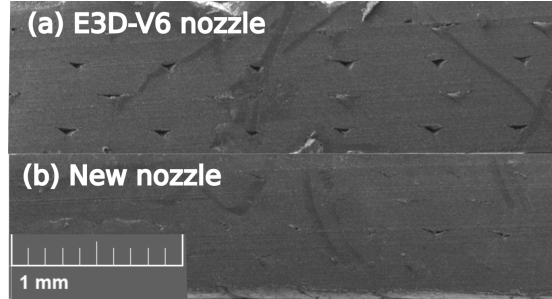
Figure 9: SEM images of a cross-section of printed walls with (a) the standard nozzle and with (b) the new nozzle (magnification 57×).

magnification of 57×. The scale bar is equal to 1 mm. The top image is taken from a sample printed with a standard nozzle while the bottom image is taken from a sample printed with the new nozzle. Note that porosity is more important in the sample printed with the standard nozzle. Gas channels are clearly visible in the sample printed with the E3D-V6 nozzle. These channels are formed at the junction between two layers of threads. These channels disappear when the samples are printed with the new nozzle. Each wall has been printed with the same printer working conditions. However, it is difficult at this stage to explain why porosity seems to differ.

Figure 10 are magnified images of the cross-sections for each printed sample with (a) the standard nozzle and (b) the new nozzle. The SEM magnification is set to 300×. As observed by Xu et al. [22] on the printing of an unique thread, the cross-section of each thread is similar to an oblong shape. This signature is well seen in the SEM image obtained on the sample printed with the new nozzle. It is easy to distinguish between the bottom and the top of each thread. The adhesion at the bottom of each thread is more important than at the top. For both printed samples, the thread height are equal to 177 μm as shown in Figure 10. This height is smaller than the gap between two layers set equal to 200 μm from the working conditions of the printer. The thread width measured in the sample obtained with the new nozzle is approximately 316 μm. For the sample printed with the standard nozzle, the width is more difficult to estimate. The typical size of the gas cavities is also shown in Figure 10. For samples printed with the E3D-V6 nozzle, the typical size is around 89 μm, while for samples printed with the new nozzle, the typical dimension is reduced by a factor of 1.7.
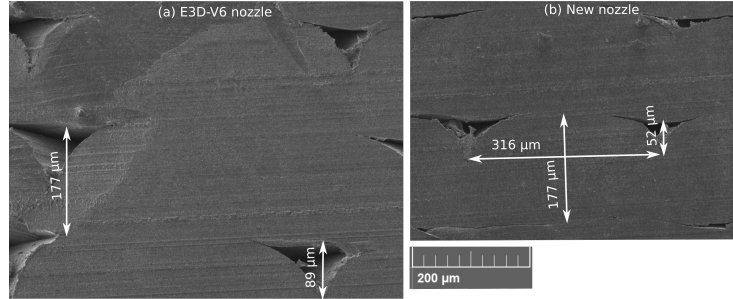
15

Figure 10: SEM images of the cross-section of printed bars with (a) the standard nozzle and with (b) the new nozzle (magnification 300×).

The density of the two samples was determined by the volumetric method. Values confirm the SEM observations. The porosity of the samples printed with a standard nozzle is equal to 10 %, while it is only equal to 7 % for the samples printed with the new nozzle. The increase in the electrical conductivity can be explained by the reduction in porosity. The overall electrical conductivity is expected to be due to the conductivity of each individual thread and the welding between them. Another explanation is that the porosity of the printed walls is related to the poor adhesion between the threads. Consequently, an increase in porosity could be an indicator of poor conductivity.

According to Fallon et al. [12], the porosity of the samples is due to a poor cohesion between threads. Fallon et al. [12] explained a decrease of contact and adhesion between threads by an increase in the dynamic viscosity of the polymer. As pinpointed in section 2, the standard nozzle results in a preferential concentration of carbon black in the capillary tube, which increases the dynamic viscosity of the composite. The increase in viscosity could have an effect on porosity in the printed parts. However, this contention needs to be confirmed by further studies.

4. Synthesis and perspectives

Printing composites using a material extrusion process is still an issue. In particular, PLA/CB composites may be useful for printing electrically conductive products. To this end, a new nozzle has been designed using computational fluid dynamics. Numerical computations were first carried out on the melting through the heat block equipped with

16

a standard nozzle provided in E3D-online. The preferential concentration of carbon black is estimated with the Q-criterion corresponding to the second invariant of the velocity gradient. The junction between the barrel of the heat block and the capillary tube at the end of the nozzle produces a large variation in the Q-criterion. It was impossible to print an object with a standard E3D-V6 nozzle, confirming the conclusion of our numerical computations. To overcome this impossibility, a new nozzle has been designed. From the numerical computations, the fluid motion and heat transfer were also studied. The new nozzle was designed by eliminating the large contraction. The study of the Q-criterion emphasizes that there is no preferential concentration of CB. A macroscopic object was printed with the new nozzle without failure. The new nozzle designed in this paper significantly improves the printability of filled polymer as it was suggested by Croom et al. [8].

The electrical properties were analyzed by printing small walls. The electrical conductivity increases significantly when samples are printed on a printer equipped with the new nozzle. SEM images show that the porosity of objects printed with the new nozzle is reduced compared to objects printed with the standard nozzle. The porosity is equal to 7 % for walls printed with the new nozzle, while it reaches 10 % for the walls printed with the standard nozzle.

The production of the proposed nozzle geometry does not require any major changes to the nozzle manufacturing process and the design could easily be adopted as a standard design for the printing of filled filaments.

Acknowledgments

Credit author statement

S. Marion: Investigation, Methodology, Validation, Formal analysis, Software, Writing - Review & Editing. **T. Joffre**: Conceptualisation, Formal analysis, Methodology, Writing - Review & Editing. **J. Jaxel**: Experimentation, Formal analysis, Writing - Review & Editing. **F. Pigeonneau**: Conceptualisation, Supervision, Investigation, Methodology, Validation, Formal analysis, Software, Writing - Original Draft.

Declaration of Competing Interest

The authors declare that they have no known competing financial interests or personal relationships that could have appeared to influence the work reported in this article.

;;

5. Divergence of the particle velocity field

To determine the divergence of the particle velocity field, the second Newton's law applied to the particle is written as follows

$$\frac{d\boldsymbol{v}_p}{dt} = \frac{\boldsymbol{u} - \boldsymbol{v}_p}{\tau_p}, \tag{7}$$

with τ_p given by (6).

Since τ_p can be considered as a small quantity, a perturbation method is used to estimate the velocity of the particles. Using an iterative procedure [23], the first order approximation gives the following approximation

$$\boldsymbol{v}_p = \boldsymbol{u} - \tau_p \frac{d\boldsymbol{u}}{dt}, \tag{8}$$

accurate at the second order in τ_p.

The divergence of the last equation in the case of divergence-free $\boldsymbol{u}$ gives the following equation

$$\boldsymbol{\nabla} \cdot \boldsymbol{v}_p = -\tau_p u_{i,j} u_{j,i} = 2\tau_p Q. \tag{9}$$

18

References

[1] A. Bandyopadhyay, K. D. Traxel, C. Koski, and S. Bose. *Additive manufacturing of polymers*, chapter 2, pages 25–42. CRC Press, 2019.

[2] S. Kirkpatrick. Percolation and conduction. *Rev. Mod. Phys.*, 45(4):574–588, 1973.

[3] D. H. Park, T. G. Kan, Y. K. Lee, and W. N. Kim. Effect of multi-walled carbon nanotube dispersion on the electrical and rheological properties of poly(propylene carbonate)/poly(lactic acid)/multi-walled carbon nanotube composites. *J. Mater. Sci.*, 48:481–488, 2013.

[4] L. C. Martins and A. Pontes. Fiber reinforced thermoplastics compounds for electromagnetic interference shielding applications. *J. Reinf. Plast. Compos.*, 41(5-6):206–214, 2022.

[5] Y. Wang and R. H. Ewoldt. New insights on carbon black suspension rheology—anisotropic thixotropy and antithixotropy. *J. Rheol.*, 66(5):937–953, aug 2022.

[6] W. Zhang, A. A. Dehghani-Sanij, and R. S. Blackburn. Carbon based conductive polymer composites. *J. Mater. Sci.*, 42(10):3408–3418, 2007.

[7] Y. Kazemi, A. R. Kakroodi, A. Ameli, T. Filleter, and C. B. Park. Highly stretchable conductive thermoplastic vulcanizate/carbon nanotube nanocomposites with segregated structure, low percolation threshold and improved cyclic electromechanical performance. *J. Mater. Chem. C*, 6(2):350–359, 2018.

[8] B. P. Croom, A. Abbott, J. W. Kemp, L. Rueschhoff, L. Smieska, A. Woll, S. Stoupin, and H. Koerner. Mechanics of nozzle clogging during direct ink writing of fiber-reinforced composites. *Addit. Manuf.*, 37:101701, 2021.

[9] S. Jang, A. Boddorff, D. J. Jang, J. Lloyd, K. Wagner, N. Thadhani, and B. Brettmann. Effect of material extrusion process parameters on filament geometry and inter-filament voids in as-fabricated high solids loaded polymer composites. *Addit. Manuf.*, 47:102313, 2021.

[10] B. P. Heller, D. E. Smith, and D. A. Jack. Effects of extrudate swell and nozzle geometry on fiber orientation in Fused Filament Fabrication nozzle flow. *Addit. Manuf.*, 12:252–264, 2016.

[11] Y. Kanarska, E. B. Duoss, J. P. Lewicki, J. N. Rodriguez, and A. Wu. Fiber motion in highly confined flows of carbon fiber and non-newtonian polymer. *J. Non-Newtonian Fluid Mech.*, 265:41–52, 2019.

[12] J. J. Fallon, S. H. McKnight, and M. J. Bortner. Highly loaded fiber filled polymers for material extrusion: A review of current understanding. *Addit. Manuf.*, 30:100810, 2019.

[13] A. Abdalla, H. H. Hamzah, O. Keattch, D. Covill, and B. A. Patel. Augmentation of conductive pathways in carbon black/pla 3d-printed electrodes achieved through varying printing parameters. *Electrochim. Acta*, 354:136618, 2020.

[14] R. Jones, P. Haufe, E. Sells, P. Iravani, V. Olliver, C. Palmer, and A. Bowyer. RepRap – the replicating rapid prototyper. *Robotica*, 29(1):177–191, 2011.

[15] E3D-online. E3d help centre. https://e3d-online.zendesk.com/hc/en-us, 2021.

[16] D. Xu, J.-F. Agassant, and F. Pigeonneau. Dimensions of the deposited strand in the material extrusion process: Experimental and numerical investigations. *Addit. Manuf.*, 59:103107, 2022.

[17] S. Marion, L. Sardo, T. Joffre, and F. Pigeonneau. First steps of the melting of an amorphous polymer through a hot-end in fused filament fabrication. *Addit. Manuf.*, 65:103435, 2023.

[18] F. Pigeonneau, D. Xu, M. Vincent, and J.-F. Agassant. Heating and flow computations of an amorphous polymer in the liquefier of a material extrusion 3d printer. *Addit. Manuf.*, 32:101001, 2020.

[19] J. Guo, C.-H. Tsou, Y. Yu, C.-S. Wu, X. Zhang, Z. Chen, T. Yang, F. Ge, P. Liu, and M. Reyes De Guzman. Conductivity and mechanical properties of carbon black-reinforced poly(lactic acid) (pla/cb) composites. *Iran. Polym. J.*, 30:1251–1262, 2021.

[20] C. Truesdell. *The kinematics of vorticity*. Indiana University Press, 1954.

[21] T. Elperin, N. Kleeorin, and I. Rogachevskii. Self-excitation of fluctuations of inertial particle concentration in turbulent fluid flow. *Phys. Rev. Lett.*, 77(27):5373–5376, 1996.

[22] D. Xu, Y. Zhang, and F. Pigeonneau. Thermal analysis of the fused filament fabrication printing process: Experimental and numerical investigations. *Int. J. Mater. Form.*, 14(4):763–776, 2021.

[23] E. J. Hinch. *Perturbation Methods*. Cambridge Univ. Press, 1991.